Int. J. Electrochem. Sci., 17 **(2022)** Article Number: 220854, doi: 10.20964/2022.08.47

International Journal of
ELECTROCHEMICAL
SCIENCE
www.electrochemsci.org

Synthesis of Graphene oxide@silicon Naocomposites and Its high-Performance as Lithium Ion Battery Anodes

Weiwei Wang[*], *Meng Tian, Feng Wu, Yujie Li*

School of Physics and New Energy, Xuzhou University of Technology, Xuzhou, 221018, China
[*]E-mail: wwwang@xzit.edu.cn

Received: 16 May 2022 / *Accepted:* 10 June 2022 / *Published:* 4 July 2022

The electrochemical characteristics of graphene oxide and Si nanocomposite (GO@Si) anode materials for lithium ion batteries were evaluated using chemo-thermal production. The structure and morphology of a GO@Si nanocomposite anode with 50% Si revealed that well-crystalline Si particles were uniformly enwrapped by graphene oxide nanosheets, forming the GO@Si nanocomposite's connection network. The first cycle discharge capacity increased from 1440 mA h/g for GO to 1471 mAh/g for Si and 1570 mAh/g for GO@Si nanocomposite at a current density of 0.5 A/g, indicating that the GO@Si nanocomposite performed better, which can be attributed to synergistic effects of the conductive GO nanosheets and the highly rough and porous structure of the nanocomposite. The conductive structure of the GO@Si nanocomposite electrode may effectively buffer the volume expansion–contraction during electrochemical cycling, according to the findings. After 300 electrochemical lithiation (discharge)/delithiation (charge) cycles, it was discovered that the GO@Si nanocomposite had excellent stability performance, with an effective capacity of 1018 mA h/g, which was roughly 3-fold that of a commercial graphite-based anode. The capacity retention of the GO@Si nanocomposite was 91% for the first 300 cycles, with a coulombic efficiency of 99.6%. The electrochemical performance of GO@Si nanocomposite containing 50% Si and different published anode materials for lithium ion batteries indicated that other anodes performed better or comparable. The rate capacity of the GO@Si nanocomposite indicated that at high current and fast rates, there was no structural degradation to the layer structure.

Keywords: Graphene oxide; GO@Si nanocomposite; Lithium Ion Batteries; Capacity retention; Cycling stability

1. INTRODUCTION

As the globe shifts away from fossil fuels and toward emissions-free electricity, batteries are becoming an increasingly important storage mechanism to help with the transition [1, 2]. Because of applications in portable devices and electric vehicles in households, health instruments, medical,

logistics and construction, firefighting and emergency, and military, demand for lithium-ion batteries to power electric vehicles and energy storage has grown at an exponential rate [3-5]. By 2030, demand is expected to climb 17-fold, lowering the cost of battery storage. The energy density of a battery refers to how much power it can store in relation to its physical size [6, 7]. Lithium ion batteries can store more energy while taking up less space than lead acid batteries, which is ideal for households with limited space [8, 9].

As a result, numerous studies have been carried out in order to improve the power density, lifetime, and safety of lithium-ion batteries [10-15]. Because of its electronic conductivity, superior cyclability, high coulombic efficiency, high energy density, and low electrochemical potential, graphite has attracted substantial interest as an anode for energy storage devices. However, lithium-ion batteries' performance is limited by their modest storage capacity (372 mA h/g) [16, 17].

Because of benefits such as its greatest known capacity and relatively low working potential, Si is also one of the most promising anode materials for mixing with or fully replacing conventional graphite anodes in lithium-ion batteries. In theory, silicon has around ten times the storage capacity of graphite [18-20]. However, before Si anodes can be used in practical lithium batteries, the problem of excessively large volumetric change and low stability must be solved [21]. Because of its high rough and nanoporous structure, which provide an ideal conductive matrix and buffer spaces for electron transfer during the lithiation process, graphene has been studied for its potential use in the composition of new batteries in recent years, and results have indicated that graphene can be considered a potential miracle material that will revolutionize lithium-ion batteries and promote lithium-ion battery performance [22-25].

In this work, the GO@Si nanocomposites were designed as an anode material for lithium-ion batteries via a simple chemo-thermal technique. GO is a promising precursor for the creation of carbon-based nanostructures because of its low cost, friendliness, and tailored properties and functionalized with plenty of hydroxyl, epoxy, and carboxyl moieties, which can facilitate the homogeneous deposition of Si nanoparticles in aqueous solution [26-28]. Moreover, the interconnected GO layers provide a matrix to buffer the volume change and a conductive network to enhance the conductivity, which leads to the improved performance. Herein, the use of chemo-thermal techniques is a simple and effective strategy for the production of firmly-bonded and uniformly dispersed GO@Si nanocomposites which can offer a large specific surface area and pathway for lithium transport and reaction, leading to better cycling and rate performance. Moreover, the stoichiometry of GO and Si nanoparticles in GO@Si nanocomposites is an important parameter which can effect lithium-ion battery performance. As a result, more research is needed to optimize synthesis methodologies, stoichiometry and mixture preparation, and hybrid and nanocompositions of Si and graphene to increase thermal, chemical, and structural stability in practical applications for cycling performance. As a result, this research focused on the chemo-thermal synthesis of GO@Si nanocomposite anode material for lithium ion batteries, as well as the electrochemical properties of the material.

2. EXPERIMENTAL

2.1. Synthesis of GO@Si nanocomposite

The chemo-thermal technique [23] was used to make the GO@Si nanocomposite. To make the GO@Si nanocomposite, a mixture of Si nanoparticles (200 nm, Sigma-Aldrich) and GO (99%, Xiamen Tob New Energy Technology Co., Ltd., China) was blended in a N-Methyl-2-pyrrolidone (NMP, ≥ 99.5%, Sigma-Aldrich) solution of poly(vinylidene fluoride) (PVDF, Sigma-Aldrich). For synthesis of the GO@Si nanocomposite, 50 wt% Si nanoparticles, 40 wt% GO, 4 wt% NMP and 6 wt% PVDF were added. The GO@Si nanocomposite was made with 40 wt% Si nanoparticles, 50 wt% GO, 4 wt% NMP and 6 wt% PVDF. The GO@Si nanocomposite was made with 60 wt% Si nanoparticles, 30 wt% GO, 4 wt% NMP and 6 wt% PVDF. To achieve a homogeneous composition, the mixture was mixed. The mixture was then ball milled in an agate vial with agate balls for 8 hours. Following the ball milling procedure, the mixes were washed three times with deionized water and vacuum dried for four hours at 95 °C. In order to carbonize PVDF and minimize GO, the composite was calcined at 650°C for 150 minutes in a tube furnace with a gas flow containing a 1:19 mixture of H_2/N_2.

2.2. Electrochemical analyses

Using a 2032 coin-type cell with lithium metal as the counter and reference electrodes, the electrochemical characteristics of the GO, Si, and GO@Si nanoomposite were investigated. A microporous polypropylene sheet separated the electrodes (Celgard 2400, Hoechst-Celanese Co., North Carolina, USA). The working electrodes were made up of 75 wt.% produced composition powder (GO, Si, and GO@Si nanoomposite), 15% acetylene black (99.5%, Shandong Gelon Lib Co., Ltd., China), and 10% carboxymethylcellulose sodium (average molecular weight of 90000, Sigma-Aldrich) as a binder. The well-blended slurry was spread over copper foil, dried for 30 minutes at 80°C, and then cooked for 120 minutes at 150°C in a vacuum oven. A solution of 1 M LiPF6 dissolved in a combination of ethylene carbonate (EC), dimethyl carbonate (DMC), and ethyl methyl carbonate (EMC) serves as the electrolyte (1:1:1 by volume). In a glove box filled with pure argon, the cell assembly was operated (99.999 percent). The total masses of Si and carbon were used to calculate the specific capacity values. A potentiostat/galvanostat was used to investigate the electrochemical characteristics (CS350, Wuhan Corrtest Instruments Corp., Ltd., China).

2.3. Morphology and Structure characterizations

The crystal structures and morphology of the synthesized compositions were studied using an X-ray diffractometer (XRD; Rigaku D/max-2400, Japan) and scanning electron microscopy (Hitachi 3000, Tokyo, Japan).

3. RESULTS AND DISCUSSION

3.1. Study the structural properties

Figure 1 shows the XRD patterns of GO, Si, and GO@Si containing 50 wt% Si. One of the characteristic diffraction peaks in the XRD pattern of the GO sample is at 2θ =11.89°, which corresponds to (002) planes of the hexagonal graphite structure of GO [29-31]. Strong diffraction peaks are observed in the XRD patterns of Si nanoparticles and GO@Si at 2θ = 24.93°, 45.49°, 55.22°, 69.27°, and 76.59°, which are attributed to the (111), (220), (311), (400), and (331) crystalline planes of face-centeredcubic structure Si (JCPDS card no. 80-0018) [32-34]. The XRD pattern of GO@Si exhibits an extra GO peak (002), showing that GO sheets are dispersed within Si nanoparticles.

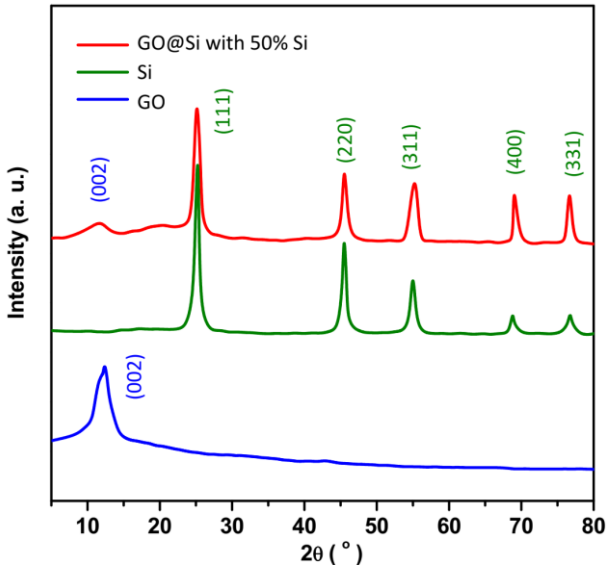

Figure 1. XRD patterns of GO, Si and GO@Si contained 50 wt% Si.

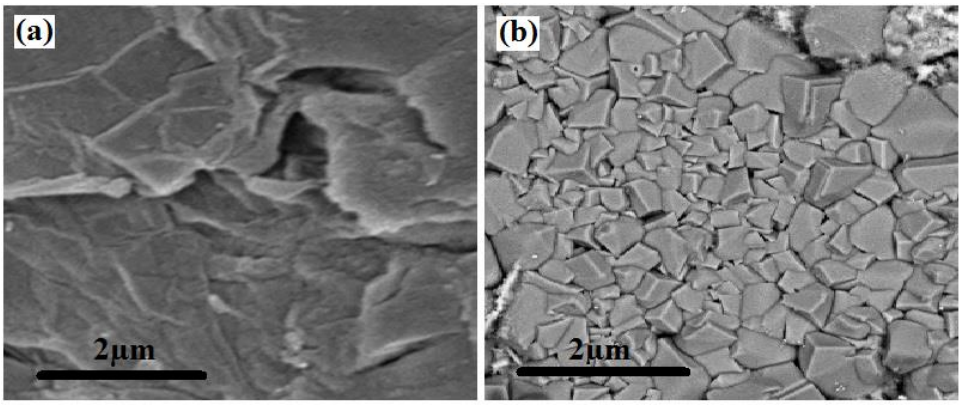

Figure 2. SEM micrographs of (a) GO and (b) GO@Si contained 50 wt% Si.

Figure 2 shows SEM micrographs of GO and GO@Si composites containing 50% Si by weight. Figure 1a exhibits multilayer nano-sized ultrathin nanosheets of GO with kinked and wrinkled nanosheets and atomically clean edges in a SEM micrograph. Figure 1b shows SEM images of the GO@Si composite, which show evenly spherical-shaped Si particles scattered on GO nanosheets in micron dimensions. Si particles are uniformly coated in graphene oxide nanosheets, forming the GO@Si nanocomposite's connection network. It has a high degree of roughness and porosity, which boosts catalytic activity and surface area.

3.2. Electrochemical analyses

Figure 3 displays the dQ/dV profiles at voltages from 0 to 2.5 V (vs. Li/Li^+) for GO and GO@Si composites containing 50 wt% Si at a scan rate of 0.1 mV/s in 1M $LiPF_6$ containing EC/DMC (1:1 v:v) during the first charge–discharge process which indicated to good agreement with the earlier reports of GO and Si based nanocomposites [35-38]. The dQ/dV profile of GO is contained typical peaks broad peaks at 0.82 V in the charge profile due to the formation of a solid electrolyte interphase (SEI) film on the nanocomposites surface [38, 39], which causes to substantial irreversible capacity because of loss of a lot of Li^+ ions [40, 41]. In the GO@Si composite electrode, two peaks at 0.51 V and 0.04 V in the charge profile and one peak at 0.44 V in the following discharge profile are observed, which associated with the phase transition between amorphous Li_xSi and amorphous Si [42-44].

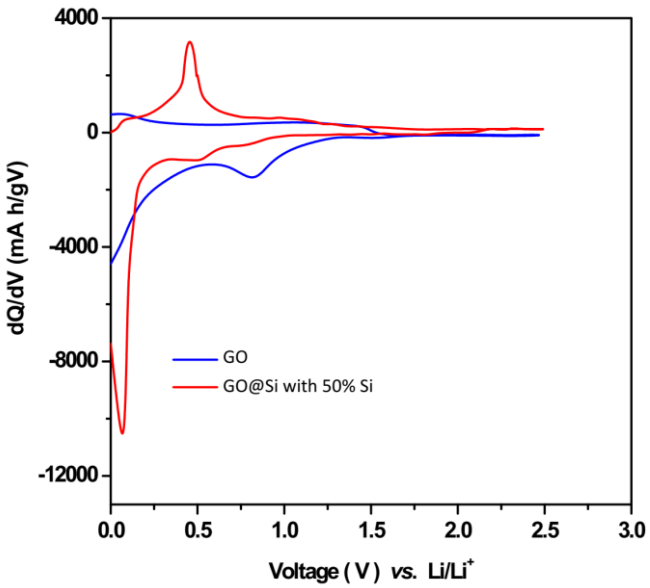

Figure 3. dQ/dV profiles at voltages from 0 to 2.5 V (vs. Li/Li^+) for GO and GO@Si composite contained 50 wt% Si at scan rate of 0.1 mV/s in 1M $LiPF_6$ containing EC/DMC (1:1 v:v).

Figure 4 shows the potential profile of GO, Si, and GO@Si nanocomposite with 50% Si at a working voltage of 0 to 2.5 V at room temperature and a current density of 0.5 A/g during the first

lithium insertion and extraction cycle (discharge and charge cycle). The first cycle discharge capacity improved from 1440 mA h/g for GO to 1471 mAh/g for Si and 1570 mAh /g for GO@Si nanocomposite, as shown in the graph. The better performance of the GO@Si nanocomposite can be attributed to the synergistic effects of the conductive GO nanosheets and the nanocomposite's high rough and porous structure, which provide an ideal conductive matrix and buffer spaces for electron transfer and Si expansion during the lithiation process [45-48].

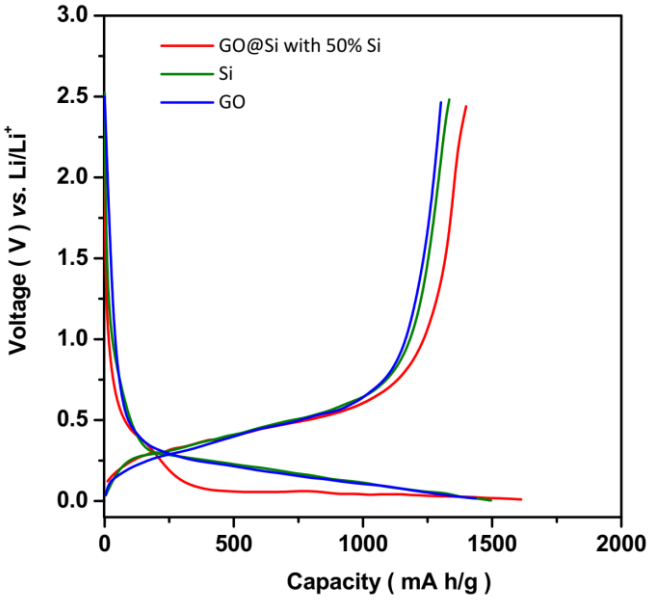

Figure 4. Potential profile in the first lithium insertion and extraction cycle (discharge and charge cycle) of GO and GO@Si nanocomposite contained 50 wt% Si under a working *voltage* from 0 to 2.5 *V* at room temperature at a current density of 0.5 A/g.

Figure 5 shows the first, second, third, and tenth charge and discharge profiles of a GO@Si nanocomposite containing 50 wt% Si at room temperature, with a working voltage of 0 to 2.5 V and a current density of 0.5 A/g. As can be seen, the GO@Si nanocomposite anode's first discharge and charge capacities are 1570 and 1370 mA h/g, respectively, resulting in a relatively low initial Coulombic efficiency of 80%, which is higher than the Coulombic efficiency reported in previous reports of GO and Si-based electrode materials [38, 49-52]. The multilayer nanocomposite matrix and wide effective surface area that contributed to the creation of the irreversible SEI layers are likely to blame for the low initial Coulombic efficiency. Another cause of the decline in early Coulombic effectiveness is the reaction between Li ions and oxygen-containing functional groups (mainly hydroxyl and epoxy groups) of GO nanosheets or SiO on the surface of Si particles [53]. The long-range plateau seen in the profile after the first lithiation stage changed into a sloping plateau, implying the electrochemical amorphization process of the crystalline Si [54-56]. Results indicate that the charge/discharge profiles are not significantly altered during further cycling, illustrating that the

conductive structure of the GO@Si nanocomposite electrode can effectively buffer the volume expansion–contraction during electrochemical cycling [57-59].

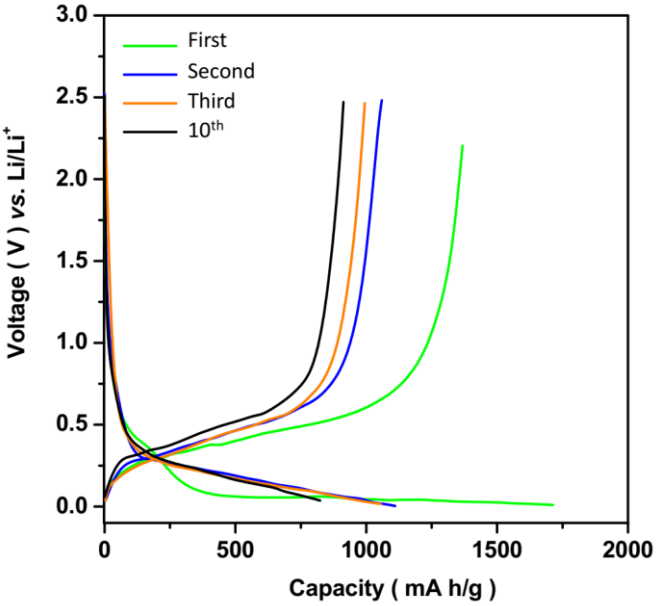

Figure 5. The first, second, third and 10th charge and discharge profiles of GO@Si nanocomposite contained 50 wt% Si under a working voltage from 0 to 2.5 V at room temperature at a current density of 0.5 A/g.

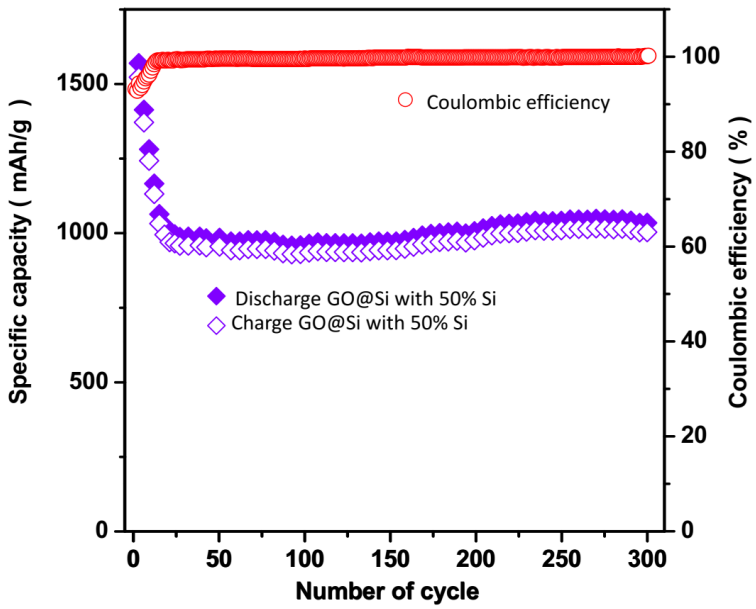

Figure 6. Capacity retention profiles and corresponding Coulombic efficiency of GO@Si nanocomposite contained 50 wt% Si electrode under a working *voltage* from 0 to 2.5 *V* at room temperature at a current density of 0.5 A/g for the 300 cycles.

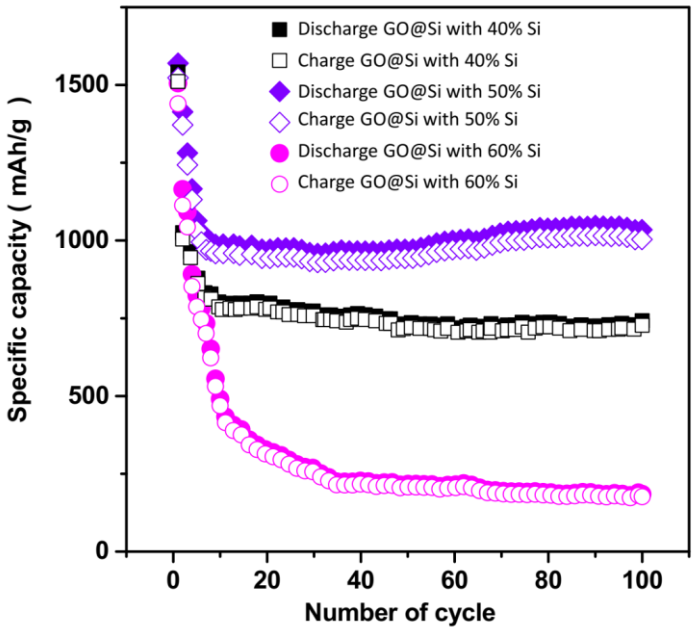

Figure 7. Specific capacities of GO@Si nanocomposite anodes with 40%, 50% and 60% Si under a working *voltage* from 0 to 2.5 *V* at room temperature at a current density of 0.5 A/g for the 100 cycles.

Figure 6 shows the stability and capacity retention curves of a GO@Si nanocomposite with a 50 wt% Si electrode after 300 cycles at room temperature with a working voltage of 0 to 2.5 V and a current density of 0.5 A/g. After 300 electrochemical lithiation (discharge)/delithiation (charge) cycles, the effective capacity of the anode is determined to be 1018 mA h/g, which is nearly 3-fold that of a commercial graphite-based anode [60-62]. The GO@Si nanocomposite exhibits excellent capacity retention for the first 300 cycles (91%). Figure 6 also shows the results of the corresponding Coulombic efficiency of the GO@Si nanocomposite electrode for 300 cycles at room temperature with a working voltage of 0 to 2.5 V and a current density of 0.5mA/g. The coulombic efficiency increased dramatically from 80.1 percent on the first cycle to more than 99.6% after 10 cycles, and it remained stable until the 260th cycle.

Figure 7 shows the specific capacities of GO@Si nanocomposite anodes with 40%, 50%, and 60% Si under a working voltage of 0 to 2.5 V at room temperature for 100 cycles at a current density of 0.5 A/g. During the first 25 cycles, both nanocomposite anodes with 40% and 50% Si had significantly higher charge/discharge capacities than nanocomposite anodes with 60% Si, suggesting that GO plays a major role in charge and discharge reactions [63, 64], and could provide better conducting/buffering networks for Si-based materials [65, 66]. GO serves as a conductive network to facilitate the collection and transportation of electrons during the cycling [67, 68]. For conventional Si electrodes, the amorphous Li_xSi alloy is formed during lithiation. Mechanically, this causes a significant internal stress gradient on the surface of Si particles, causing swelling of the electrode and pulverization of Si particles [69, 70]. As consequence, The swelling and pulverization can create crack and peel off in electrode, followed by the loss of electrical contact between Si particles and current collector, and generate of nonactive Si and poor electrical conductivity, and discontinuous current

pathway [69, 71, 72]. In GO@Si nanocomposite, the entrapment of the Si nanoparticles by GO nanosheets protects Si nanoparticles from direct exposure to the electrolyte during lithiation/delithiation processes, and promotes Coulombic efficiency and stability of the electrode [73, 74]. Furthermore, while the first discharge capacity of the nanocomposite anode with 50% Si (1570 mA h/g) is slightly higher than that of the nanocomposite anode with 40% Si (1541 mA h/g), the retained charge capacity of the anode with 50% Si (1490 mA h/g) is higher than that of the anode with 40% Si (1004 mA h/g). As a result, the initial coulombic efficiency of the 50% Si nanocomposite anode is roughly 94%. This number is higher than the 40% Si anode value (65%). It has been suggested that a low initial coulombic efficiency is associated with a decrease in the capacity of the electrode which is related to the consumption of Li ions trapped in the nanoporous matrix of GO@Si nanocomposite, and also the irreversible reaction of Li ions and the creation of a solid SEI layer on the nanocomposite at voltages lower than 1.0 V (vs. Li/Li^+) [75, 76]. As seen, the lithiation/delithiation capacities of anodes with 40% and 50% Si are approximately similar in the first 10 cycles, the specific capacity of an anode with 40% Si drops significantly during further cycling, and it reaches 731 mA h/g after 100 cycles. For anodes with 50% Si, the specific capacity is slightly increased after 100 cycles and gets to 1051 mA h/g which is significantly higher than anodes with 40% and 60% Si. Therefore, the GO@Si nanocomposite anode with 50% Si shows the good wrapping effect of Si particles by GO nanosheets which forms a stable and efficient conducting/buffering framework.

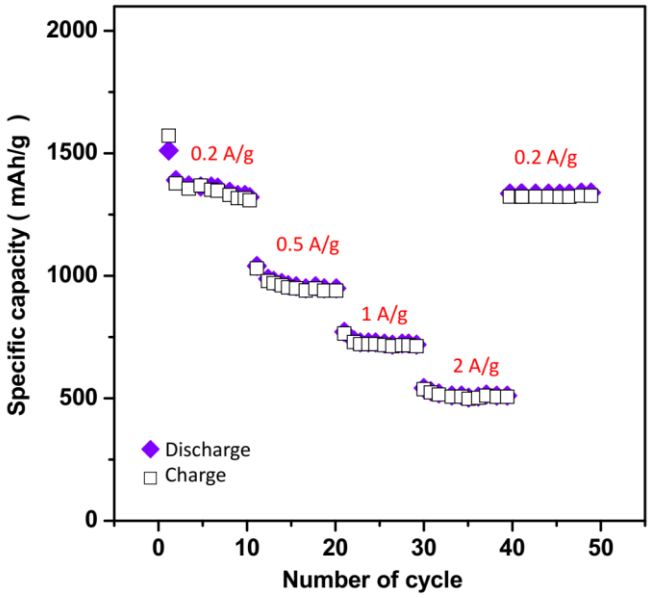

Figure 8. Rate capability of GO@Si nanocomposite contained 50 wt% Si electrode under a working voltage from 0 to 2.5 V at room temperature at various current densities from 0.2 to 2 A/g for the 50 cycles.

Figure 8 shows the rate capability of a GO@Si nanocomposite including a 50wt% Si electrode for 50 cycles at room temperature with a working voltage ranging from 0 to 2.5 V and current densities ranging from 0.2 to 2 A/g. As can be shown, the discharge capacities reach 1376 mA h/g at 0.2 A/g

after the first 10 cycles, 1050 mA h/g after the second 10 cycles, 756 mA h/g after the third 10 cycles, and 519 mA h/g after the second 10 cycles (between 30th and 40th cycles). Furthermore, when the current rate is reduced to 0.2 A/g (between the 40th and 50th cycles), the capabilities of Si nanocomposite are restored to their initial values, suggesting that there is no structural degradation to the layer structure at high current and fast rates. Table 1 exhibits the comparison between the electrochemical performance of the GO@Si nanocomposite containing 50 wt% Si and various reported anode materials for lithium ion batteries. It is found that GO@Si nanocomposite containing 50 wt% Si anode shows better or comparable performance to other anodes presented in Table 1.

Table 2. Comparision beween the electrochemical performance of GO@Si nanocomposite contained 50 wt% Si and varoius reported anode materials for lithium ion batteries.

Composition	**voltage range (V)**	**Discharge capacity (mA h/g/)**	**Capacity retention (%)**	**Ref.**
3-D Si/carbon nanofiber	0–1.5	1957 (2 A/g)	60.6% (400 cycles) at 2 A/g	[10]
Si/C nanosphere	0–3.0	472 (1 A/g)	78% (400 cycles) at 1 A/g	[11]
SiO_x/CNT composite	0.01-3.0	1240 (0.1 A/g)	33.9% (50 cycles) at 0.5 A/g	[15]
CNT-Ni-Si	0.01-1.2	1960 (0.84 A/g)	78% (110 cycles) at 0.84 A/g	[12]
Si-rGO	0.075-2.0	750 (0.05 A/g)	100% (100 cycles) at 0.05 A/g	[13]
Liquid-exfoliated pristine graphene/Si composites	0.01–2.0	700 (1.6 A/g)	85% (100 cycles) at 1.6 A/g	[14]
GO@Si nanocomposite contained 50 wt% Si	0.0–2.5	1570 (0.5 A/g)	91% (300 cycles) at 0.5 A/g	This study

4. CONCLUSION

In summary, the structural and electrochemical properties of the GO@Si nanocomposite anode material for lithium ion batteries were synthesized and characterized in this study. The GO@Si nanocomposite was synthesized using the chemo-thermal technique. The structure and morphology of a GO@Si nanocomposite anode with 50% Si revealed that well-crystalline Si particles were uniformly enwrapped by graphene oxide nanosheets, forming the GO@Si nanocomposite's connection network. At a current density of 0.5 A/g, electrochemical characterization revealed that the first cycle discharge capacity increased from 1440 mA h/g for GO to 1471 mAh /g for Si and 1570 mAh/g for GO@Si nanocomposite, indicating that the GO@Si nanocomposite showed better performance. This is due to the synergistic effects of the conductive GO nanosheets and the nanomaterial's high rough and porous structure. The conductive structure of the GO@Si nanocomposite electrode may effectively buffer the volume expansion–contraction during electrochemical cycling, according to the findings. After 300 electrochemical lithiation (discharge)/delithiation (charge) cycles, it was discovered that the GO@Si

nanocomposite had excellent stability performance, with an effective capacity of 1018 mA h/g, which was around 3-fold that of a commercial graphite-based anode. For the first 300 cycles, the GO@Si nanocomposite showed outstanding capacity retention (91%) and coulombic efficiency of over 99.6%. The electrochemical performance of the GO@Si nanocomposite, which contains 50% Si, and several reported anode materials for lithium ion batteries, indicates that other anodes perform better or similarly. At high current and fast rates, the GO@Si nanocomposite showed no structural damage to the layer structure.

ACKNOWLEDGMENTS
The research is supported by the National Natural Science Foundation of China: The study on Schwinger effect based on entangled states in open system 11947042.

References

1. E. Derkenbaeva, S.H. Vega, G.J. Hofstede and E. Van Leeuwen, *Renewable and Sustainable Energy Reviews*, 153 (2022) 111782.
2. X. Zhang, Y. Tang, F. Zhang and C.S. Lee, *Advanced energy materials*, 6 (2016) 1502588.
3. T. Kim, W. Song, D.-Y. Son, L.K. Ono and Y. Qi, *Journal of materials chemistry A*, 7 (2019)
4. M. Wang, C. Jiang, S. Zhang, X. Song, Y. Tang and H.-M. Cheng, *Nature chemistry*, 10 (2018) 667.
5. H. Karimi-Maleh, H. Beitollahi, P.S. Kumar, S. Tajik, P.M. Jahani, F. Karimi, C. Karaman, Y. Vasseghian, M. Baghayeri and J. Rouhi, *Food and Chemical Toxicology*, (2022) 112961.
6. Z. Feng, G. Li, X. Wang, C.J. Gómez-García, J. Xin, H. Ma, H. Pang and K. Gao, *Chemical Engineering Journal*, 445 (2022) 136797.
7. M. Yang, C. Li, Z. Said, Y. Zhang, R. Li, S. Debnath, H.M. Ali, T. Gao and Y. Long, *Journal of Manufacturing Processes*, 71 (2021) 501.
8. A. Manthiram, *Nature communications*, 11 (2020) 1.
9. M. Khosravi, *Health Psychology Research*, 8 (2020) 91.
10. S.-J. Kim, M.-C. Kim, S.-B. Han, G.-H. Lee, H.-S. Choe, S.-H. Moon, D.-H. Kwak, S. Hong and K.-W. Park, *Journal of Industrial and Engineering Chemistry*, 49 (2017) 105.
11. Z. Li, Z. Li, W. Zhong, C. Li, L. Li and H. Zhang, *Chemical Engineering Journal*, 319 (2017) 1.
12. C. Lu, Y. Fan, H. Li, Y. Yang, B.K. Tay, E. Teo and Q. Zhang, *Carbon*, 63 (2013) 54.
13. C. Botas, D. Carriazo, W. Zhang, T. Rojo and G. Singh, *ACS Applied Materials & Interfaces*, 8 (2016) 28800.
14. H. Liu, Z. Shen, S. Liang, L. Liu, M. Yi, X. Zhang and S. Ma, *New Journal of Chemistry*, 40 (2016) 7053.
15. W. Guo, X. Yan, F. Hou, L. Wen, Y. Dai, D. Yang, X. Jiang, J. Liu, J. Liang and S.X. Dou, *Carbon*, 152 (2019) 888.
16. T. Bashir, S.A. Ismail, Y. Song, R.M. Irfan, S. Yang, S. Zhou, J. Zhao and L. Gao, *Energy Materials*, 1 (2021)
17. H. Karimi-Maleh, C. Karaman, O. Karaman, F. Karimi, Y. Vasseghian, L. Fu, M. Baghayeri, J. Rouhi, P. Senthil Kumar and P.-L. Show, *Journal of Nanostructure in Chemistry*, (2022) 1.
18. X. Zhang, X. Qiu, D. Kong, L. Zhou, Z. Li, X. Li and L. Zhi, *ACS nano*, 11 (2017) 7476.
19. T. Gao, Y. Zhang, C. Li, Y. Wang, Q. An, B. Liu, Z. Said and S. Sharma, *Scientific reports*, 11 (2021) 1.
20. K. Abbasi, M. Hazrati, A. Mohammadbeigi, J. Ansari, M. Sajadi, A. Hosseinnazzhad and E. Moshiri, *Indian Journal of Medical and Paediatric Oncology*, 37 (2016) 227.

21. M. Liu, C. Li, Y. Zhang, Q. An, M. Yang, T. Gao, C. Mao, B. Liu, H. Cao and X. Xu, *Frontiers of Mechanical Engineering*, 16 (2021) 649.
22. X. Cai, L. Lai, Z. Shen and J. Lin, *Journal of Materials Chemistry A*, 5 (2017) 15423.
23. D. Chen, R. Yi, S. Chen, T. Xu, M.L. Gordin and D. Wang, *Solid State Ionics*, 254 (2014) 65.
24. Y. Ren, H. Wei, X. Huang and J. Ding, *International Journal of Electrochemical Science*, 9 (2014) 7784.
25. M. Khosravi, *Journal of Eating Disorders*, 8 (2020) 1.
26. M. Yusuf, M. Kumar, M.A. Khan, M. Sillanpää and H. Arafat, *Advances in colloid and interface science*, 273 (2019) 102036.
27. R. Savari, J. Rouhi, O. Fakhar, S. Kakooei, D. Pourzadeh, O. Jahanbakhsh and S. Shojaei, *Ceramics International*, 47 (2021) 31927.
28. M.-R. Wang, L. Deng, G.-C. Liu, L. Wen, J.-G. Wang, K.-B. Huang, H.-T. Tang and Y.-M. Pan, *Organic letters*, 21 (2019) 4929.
29. Y. Chen, N. Du, H. Zhang and D. Yang, *RSC Advances*, 5 (2015) 46173.
30. J. Liu, Y. Yin, K. Wang, P. Wei, H. Lu, C. Song, Q. Liang and W. Huang, *Iscience*, 25 (2022) 104090.
31. M. Khosravi, *Pharmacopsychiatry*, 55 (2022) 16.
32. D.-W. Jung, K.-H. Kim, J. Lee, B.-S. Kong and E.-S. Oh, *Journal of Nanoscience and Nanotechnology*, 13 (2013) 7855.
33. C. Xin, L. Changhe, D. Wenfeng, C. Yun, M. Cong, X. Xuefeng, L. Bo, W. Dazhong, H.N. LI and Y. ZHANG, *Chinese Journal of Aeronautics*, (2021) 1.
34. R.S. Moghadam, M. Akbari, Y. Alizadeh, A. Medghalchi and R. Dalvandi, *Middle East African Journal of Ophthalmology*, 26 (2019) 11.
35. L. Gan, H. Guo, Z. Wang, X. Li, W. Peng, J. Wang, S. Huang and M. Su, *Electrochimica Acta*, 104 (2013) 117.
36. W. Liu, H. Xu, H. Qin, Y. Lv, F. Wang, G. Zhu, F. Lin, L. Wang and C. Ni, *Journal of Solid State Electrochemistry*, 23 (2019) 3363.
37. Y. Chen, X. Zhang, Y. Tian and X. Zhao, *Journal of Nanomaterials*, 2014 (2014) 734751.
38. H.-C. Tao, L.-Z. Fan, Y. Mei and X. Qu, *Electrochemistry Communications*, 13 (2011) 1332.
39. H. Karimi-Maleh, R. Darabi, M. Shabani-Nooshabadi, M. Baghayeri, F. Karimi, J. Rouhi, M. Alizadeh, O. Karaman, Y. Vasseghian and C. Karaman, *Food and Chemical Toxicology*, 162 (2022) 112907.
40. M.-S. Wang, Z.-Q. Wang, R. Jia, Y. Yang, F.-Y. Zhu, Z.-L. Yang, Y. Huang, X. Li and W. Xu, *Applied Surface Science*, 456 (2018) 379.
41. A. Medghalchi, M. Akbari, Y. Alizadeh and R.S. Moghadam, *Journal of current ophthalmology*, 30 (2018) 353.
42. C. Guo, D. Wang, Q. Wang, B. Wang and T. Liu, *International Journal of Electrochemical Science*, 7 (2012) 8745.
43. Y. Gu, S. Yang, G. Zhu, Y. Yuan, Q. Qu, Y. Wang and H. Zheng, *Electrochimica Acta*, 269 (2018) 405.
44. Z. Huang, P. Luo, H. Zheng and Z. Lyu, *Journal of Alloys and Compounds*, 908 (2022) 164599.
45. W. Li, Y. Tang, W. Kang, Z. Zhang, X. Yang, Y. Zhu, W. Zhang and C.S. Lee, *Small*, 11 (2015) 1345.
46. Z. Li, H. Li, X. Zhu, Z. Peng, G. Zhang, J. Yang, F. Wang, Y.F. Zhang, L. Sun and R. Wang, *Advanced Science*, 9 (2022) 2105331.
47. S. Guo, C. Li, Y. Zhang, Y. Wang, B. Li, M. Yang, X. Zhang and G. Liu, *Journal of Cleaner Production*, 140 (2017) 1060.
48. A. Baradaran-Rafii, M. Akbari, E. Shirzadeh and M. Shams, *Journal of ophthalmic & vision research*, 10 (2015) 90.

49. E. Park, H. Yoo, J. Lee, M.-S. Park, Y.-J. Kim and H. Kim, *Acs Nano*, 9 (2015) 7690.
50. F. Wang, G. Chen, N. Zhang, X. Liu and R. Ma, *Carbon Energy*, 1 (2019) 219.
51. S.-L. Chou, J.-Z. Wang, M. Choucair, H.-K. Liu, J.A. Stride and S.-X. Dou, *Electrochemistry Communications*, 12 (2010) 303.
52. J. Wang, L. Liao, H.R. Lee, F. Shi, W. Huang, J. Zhao, A. Pei, J. Tang, X. Zheng and W. Chen, *Nano Energy*, 61 (2019) 404.
53. C. Chae, H.J. Noh, J.K. Lee, B. Scrosati and Y.K. Sun, *Advanced Functional Materials*, 24 (2014) 3036.
54. S.-H. Park, D. Ahn, Y.-M. Choi, K.C. Roh and K.-B. Kim, *Journal of Materials Chemistry A*, 3 (2015) 20935.
55. H. Maleh, M. Alizadeh, F. Karimi, M. Baghayeri, L. Fu, J. Rouhi, C. Karaman, O. Karaman and R. Boukherroub, *Chemosphere*, (2021) 132928.
56. S. Haddadi, R. Shahrokhirad, M.M. Ansar, S. Marzban, M. Akbari and A. Parvizi, *Anesthesiology and pain medicine*, 8 (2018)
57. M.A. Rahman, G. Song, A.I. Bhatt, Y.C. Wong and C. Wen, *Advanced Functional Materials*, 26 (2016) 647.
58. J. Wang, C. Gao, Z. Yang, M. Zhang, Z. Li and H. Zhao, *Carbon*, 192 (2022) 277.
59. W. Qiao, Z. Li, W. Liu and E. Liu, *International Journal of Energy Research*, 46 (2022) 1766.
60. X. Zhou, H. Xie, X. He, Z. Zhao, Q. Ma, M. Cai and H. Yin, *Energy & Environmental Materials*, 3 (2020) 166.
61. T. Gao, C. Li, Y. Zhang, M. Yang, D. Jia, T. Jin, Y. Hou and R. Li, *Tribology International*, 131 (2019) 51.
62. M. Akbari, R. Moghadam, R. Elmi, A. Nosrati, E. Taghiabadi and N. Aghdami, *Journal of Ophthalmic and Vision Research*, 14 (2019) 400.
63. X. Zhou, L. Xu and X. Ma, *Materials Research Express*, 4 (2017) 075511.
64. J. Rouhi, H.K. Malayeri, S. Kakooei, R. Karimzadeh, S. Alrokayan, H. Khan and M.R. Mahmood, *International Journal of Electrochemical Science*, 13 (2018) 9742.
65. Y. Jiang, F. Xiang, S. Fan and Z. Sun, *New Journal of Chemistry*, 45 (2021) 21591.
66. M. Kim, H.M. Hwang, G.H. Park and H. Lee, *FlatChem*, 6 (2017) 48.
67. Y. Chen, M. Zhuo, J. Deng, Z. Xu, Q. Li and T. Wang, *Journal of Materials Chemistry A*, 2 (2014) 4449.
68. C. Liu and J. Rouhi, *RSC Advances*, 11 (2021) 9933.
69. C. Zhang, F. Wang, J. Han, S. Bai, J. Tan, J. Liu and F. Li, *Small Structures*, 2 (2021) 2100009.
70. W. Qiao, Y. Wang, J. Zhang, W. Tian, Y. Tian and Q. Yang, *Journal of Environmental Management*, 289 (2021) 112438.
71. J.R. Szczech and S. Jin, *Energy & Environmental Science*, 4 (2011) 56.
72. M. Akbari and R. Elmi, *Case reports in medicine*, 2017 (2017) 1.
73. S.-H. Park, H.-K. Kim, S.-B. Yoon, C.-W. Lee, D. Ahn, S.-I. Lee, K.C. Roh and K.-B. Kim, *Chemistry of Materials*, 27 (2015) 457.
74. L. Nan, C. Yalan, L. Jixiang, O. Dujuan, D. Wenhui, J. Rouhi and M. Mustapha, *RSC Advances*, 10 (2020) 27923.
75. B. Huang, T. Huang, L. Wan and A. Yu, *ACS Sustainable Chemistry & Engineering*, 9 (2021) 648.
76. H. Sun, G. Xin, T. Hu, M. Yu, D. Shao, X. Sun and J. Lian, *Nature communications*, 5 (2014) 1.